

**Enhanced proton conductivity of a MOF-808 framework through  
anchoring organic acids to the zirconium clusters by postsynthetic  
modification**

Xing Meng, Hai-Ning Wang,\* Lu-Song Wang, Yan-Hong Zou, and Zi-Yan Zhou\*

*School of Chemistry and Chemical Engineering, Shandong University of Technology,*

*Zibo, Shandong, 255049, P. R. China.*

\*Corresponding author

Email:wanghn913@foxmail.com; zyzhou@sdut.edu.cn

## ***Experimental Section***

### **Materials and Measurements**

All starting materials and solvents were reagent grade, commercially available and used without further purification. TG analyses were performed on a Netzsch STA449F3 analyser heated from room temperature to 900 °C at a rate of 10 °C min<sup>-1</sup>. Powder X-ray diffraction (PXRD) were recorded on Rigaku D/Max 2500/PC diffractometer at 40 kV, 100 mA with a Cu-target tube and a graphite monochromator. Infrared spectrum using the KBr pellet was measured on a Bruker Tensor 27. Nitrogen adsorption-desorption isotherms were measured at 77 K on a Autosorb IQ2 adsorptometer (Quantachrome Instruments), and water vapor adsorption isotherms were measured at 298 K. Elemental analysis (EA) were conducted using an Elementar vario EL III analyzer. X-ray photoelectron spectroscopy (XPS) was used a K-Alpha instrument from Thermo Scientific equipped with an Al K $\alpha$  microfocused X-ray source and the C1s peak at 284.6 eV as internal standard. The morphology analysis of the synthesized samples was collected on a scanning electron microscope (SEM, quanta 250). solid-state nuclear magnetic resonance spectroscopic were measured with AVANCE III 400 WB spectrometer. The proton conductivity was measured using an impedance/gain-phase analyzer (Solartron S1 1260) over a frequency range from 0.1 Hz to 1 MHz with an input alternating current (AC) voltage of 3000 mV.

**Synthesis of MOF-808:** Microcrystalline powder samples of MOF-808 were prepared according to the reported procedures<sup>1,2</sup>. H<sub>3</sub>BTC (0.21 g, 1 mmol) and ZrOCl<sub>2</sub>·8H<sub>2</sub>O (0.97 g, 3 mmol) were dissolved in DMF/formic acid (45 mL/45 mL) and placed in a Parr Teflon-lined stainless steel vessel (100 mL) under autogenous pressure, which was heated to 130 °C for two days. A white precipitate was collected by filtration and washed three times with 20 mL of fresh DMF. As-synthesized MOF-808 was then immersed in 100 mL of anhydrous DMF for three days, during which time the DMF was replaced three times per day. The DMF-exchanged compound was filtrated off and immersed in 100 mL of water for three days, during which time the

water was replaced three times per day. Water exchanged material was then immersed in 100 mL of anhydrous acetone for three days, during which time the acetone was replaced three times per day. The acetone-exchanged sample was then evacuated at room temperature for 24 h and at 150 °C for 24 h to yield activated sample.

**Synthesis of MOF-808-EDTA:** about 0.100g of activated MOF-808 was added to 1.860 g of EDTA-2Na in a solution containing 50 ml of water. The contents were placed in a 100 ml screw-capped glass jar, which was heated to 60 °C for 24 h. A white precipitate was obtained by filtration and washed with water for several times to remove unreacted EDTA. Subsequently, the solid sample was immersed in fresh acetone to exchange water in the pores of MOF-808-EDTA and this procedure was repeated for several times. The solid was then dried at 60 °C overnight under vacuum condition.

**Synthesis of MOF-808-OX:** Activated MOF-808 (0.100 g) and oxalic acid (0.800 g) were immersed in 10 ml DMF solution. The mixture was placed in a 20 ml screw-capped glass jar, which was heated to 60 °C for 24 h. A white precipitate was collected by filtration and washed with DMF and acetone for several times. The resultant solid was then dried at 60 °C over night under vacuum condition. MOF-808-EDTA sample exhibits a new peak at 1267  $\text{cm}^{-1}$ , which is consistent with N-H stretching vibration (Fig. S3).

MOF-808-OX sample exhibits a new peak at 1715  $\text{cm}^{-1}$ , which is consistent with the stretching frequency of free -COOH groups (Fig. S4).

**Synthesis of MOF-808-OX@PVA composite membranes:** PVA (1g) was dissolved in 15 mL of boiling water under stirring. After three hours, a clear solution was obtained. MOF-808-OX was sufficiently ground. Afterwards, a certain amount of (100 mg, 33.3 mg, 20 mg, and 14.3mg) the MOF-808-OX powder was added to the 1.5 mL PVA solution, and then stirred for 0.5 h at room temperature. The mixed solution was dripped onto actinic glass panes and dried at room temperature for 2 to 3 days. A series of composite membranes were obtained named MOF-808-OX@PVA-X (X = 1, 3, 5, or 7), X was the weight percentage ratio of the PVA compared with the MOF-808-OX micron-sized powder weight.

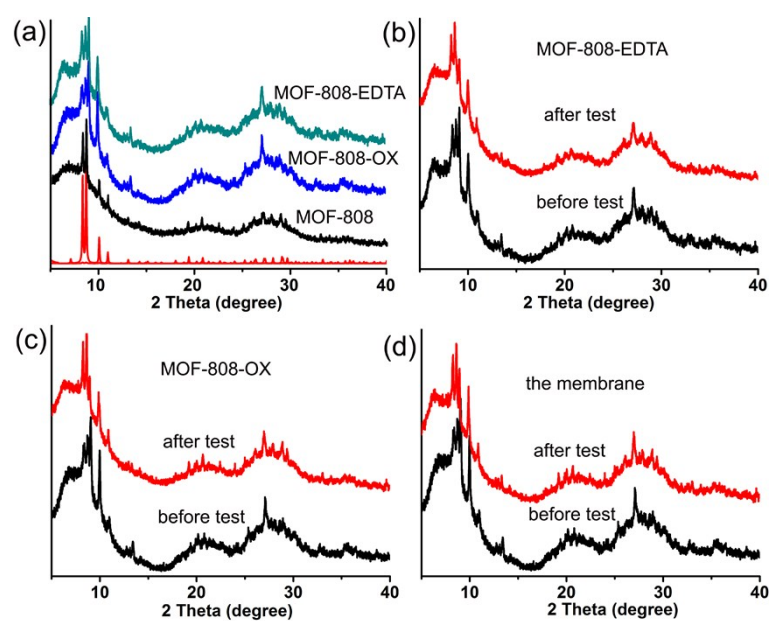


**Fig. S1** (a) PXRD patterns of simulated MOF-808, as-synthesized of MOF-808, MOF-808-EDTA and MOF-808-OX; The PXRD patterns of MOF-808-EDTA (b), MOF-808-OX (c), and MOF-808-OX@PVA-3 composite membrane (d) before and after proton conductive test.

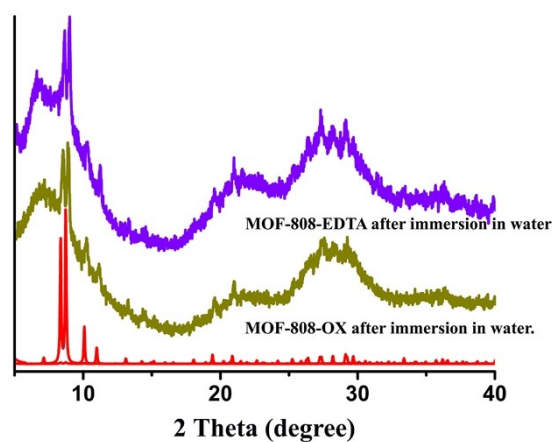
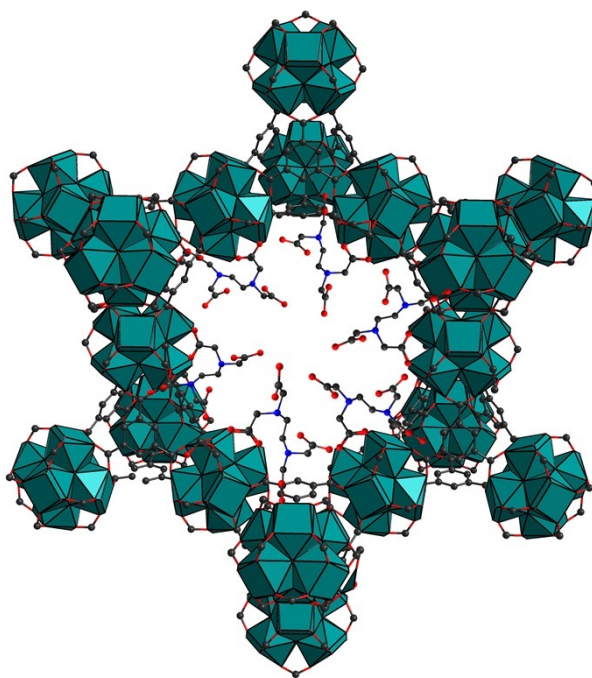


**Fig. S2** The PXRD patterns of MOF-808-EDTA and MOF-808-OX after immersion in water.



**Scheme S1** The plausible binding mode of MOF-808-EDTA.

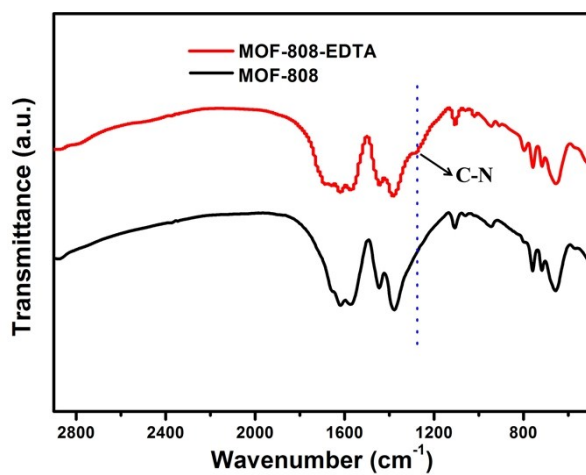


**Fig. S3** IR spectra of MOF-808 and MOF-808-EDTA.

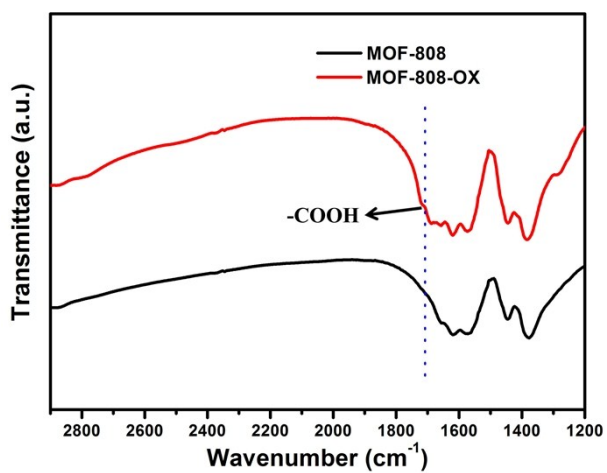


**Fig. S4** IR spectra of MOF-808 and MOF-808-OX.

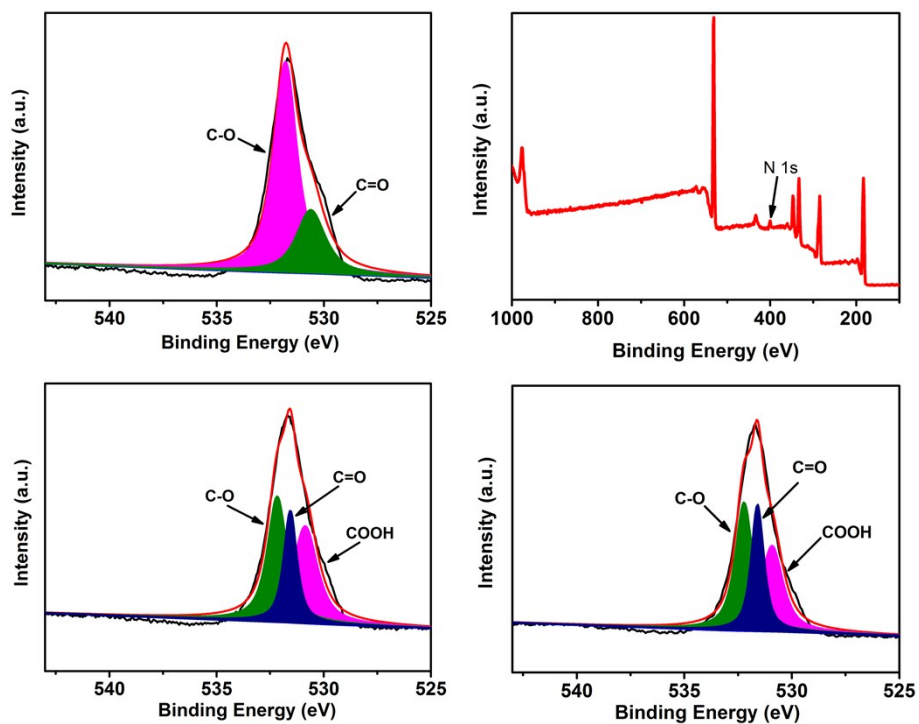


**Fig. S5** (a) XPS spectra of O1s in MOF-808; (b) XPS spectra of MOF-808-EDTA; (c) O1s in MOF-808-EDTA; and (d) O1s in MOF-808-OX.

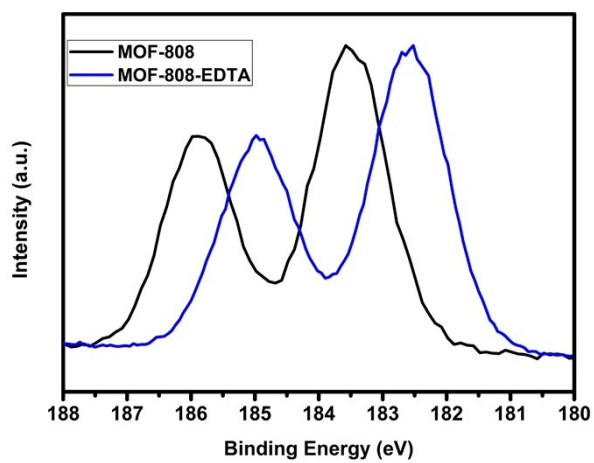


**Fig. S6** Zr 3d XPS spectra of MOF-808 and MOF-808-EDTA.

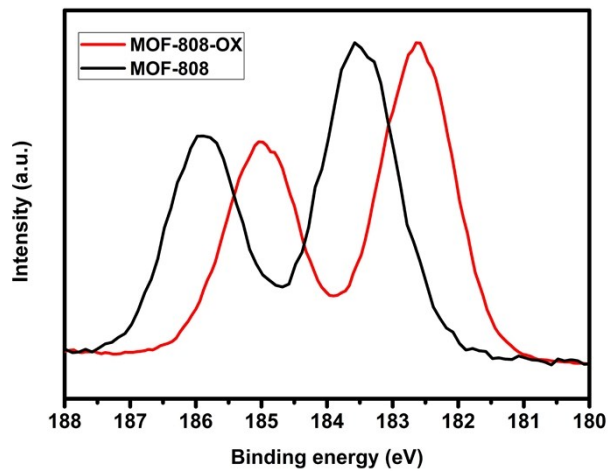


**Fig. S7** Zr 3d XPS spectra of MOF-808 and MOF-808-OX.

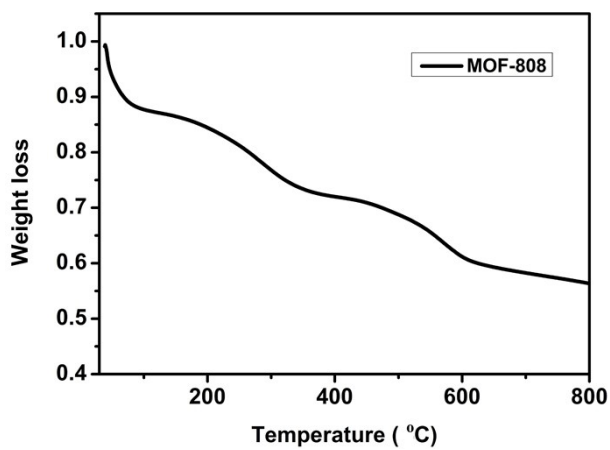


**Fig. S8** The TGA curve of MOF-808.

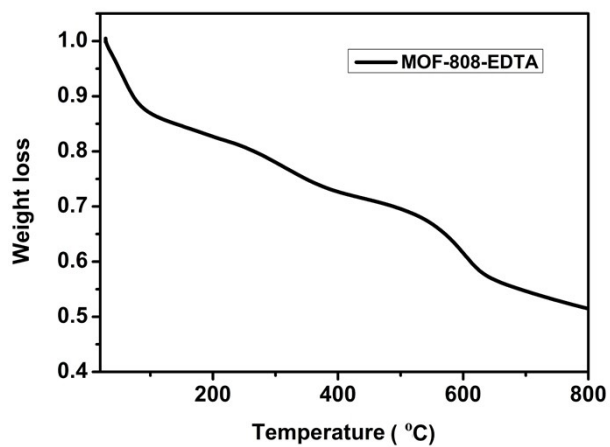


**Fig. S9** The TGA curve of MOF-808-EDTA.

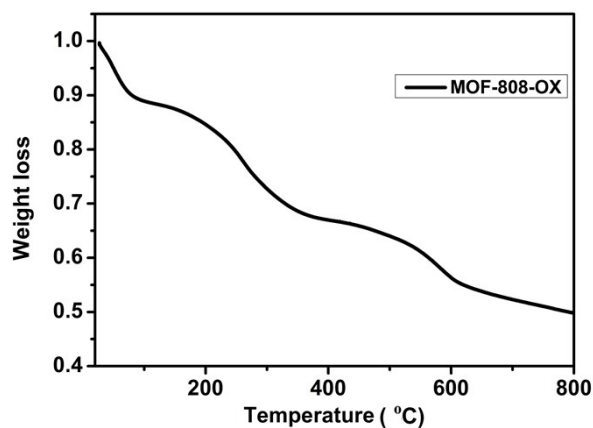


**Fig. S10** The TGA curve of MOF-808-OX.

**Table S1** Results of elemental analyses for C, N and O of MOF-808, MOF-808-EDTA, and MOF-808-OX.

Samples	C (%)	N (%)	O (%)
MOF-808	18.05	1.45	27.64
MOF-808-EDTA	19.95	2.15	27.34
MOF-808-OX	16.65	0.64	28.27

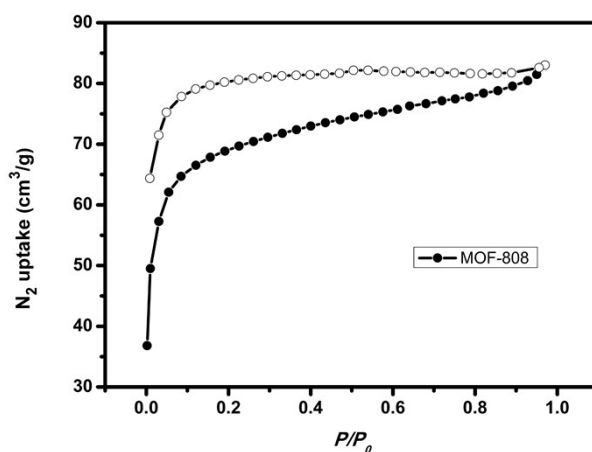


**Fig. S11** N<sub>2</sub> adsorption-desorption isotherms of MOF-808 at 77 K.

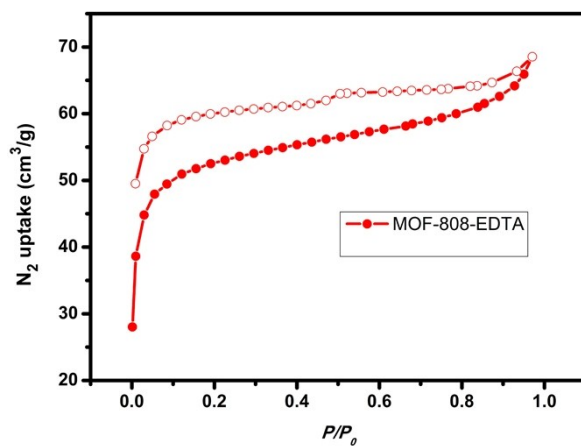


**Fig. S12** N<sub>2</sub> adsorption-desorption isotherms of MOF-808-EDTA at 77 K.

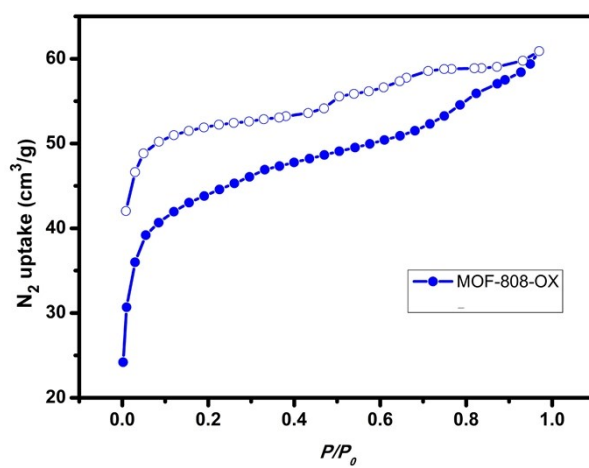


**Fig. S13** N<sub>2</sub> adsorption-desorption isotherms of MOF-808-OX at 77 K.

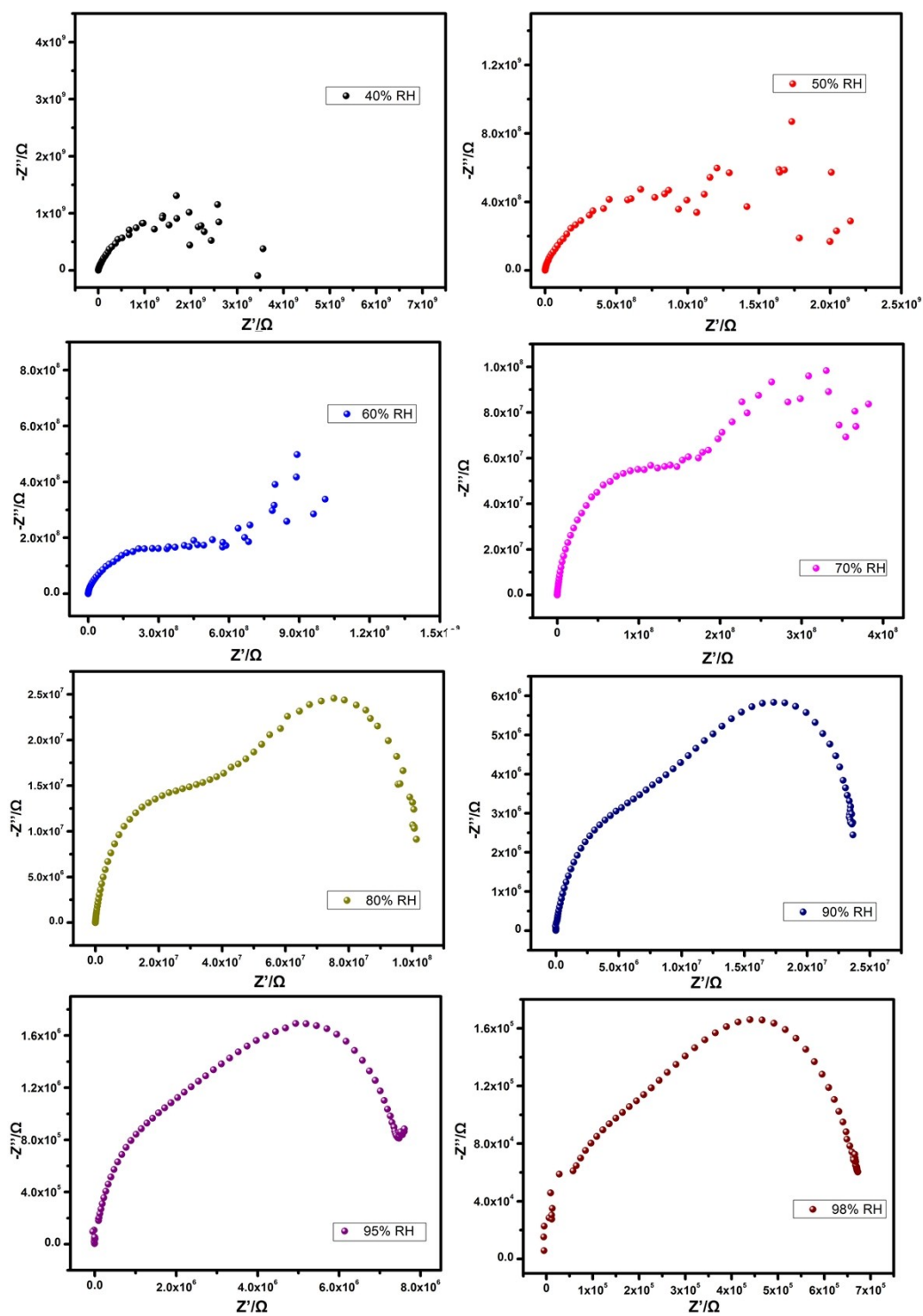


**Fig. S14** Impedance spectra of MOF-808 at 30°C with different RHs.

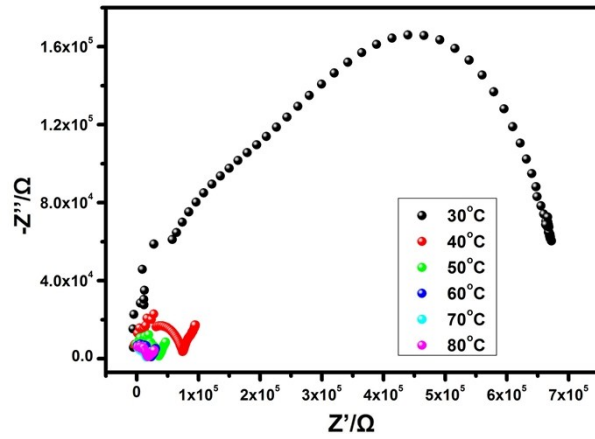


**Fig. S15** Impedance spectra of MOF-808 with 98% RH under different temperature.

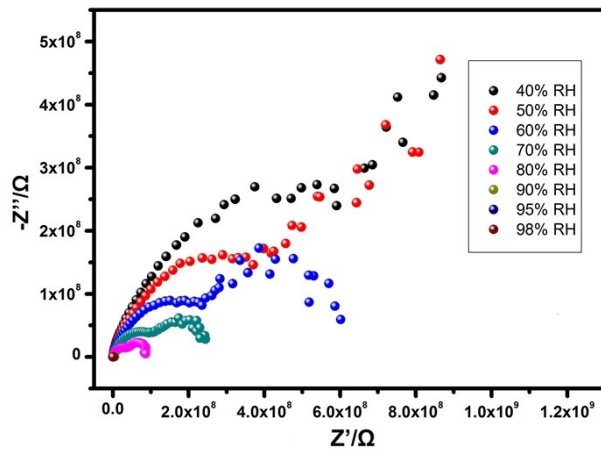


**Fig. S16** Impedance spectra of MOF-808-EDTA at 30°C with different RHs.

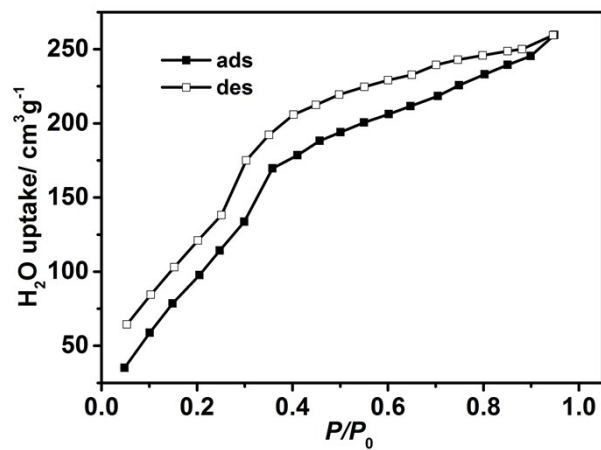


**Fig. S17** Water vapor adsorption and desorption isotherms of MOF-808.

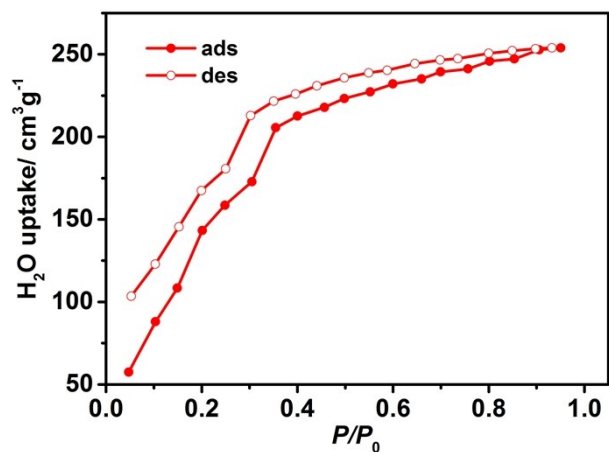


**Fig. S18** Water vapor adsorption and desorption isotherms of MOF-808-EDTA.

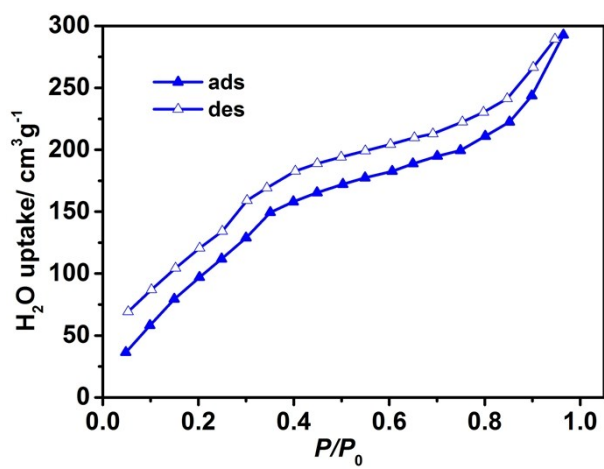


**Fig. S19** Water vapor adsorption and desorption isotherms of MOF-808-OX.

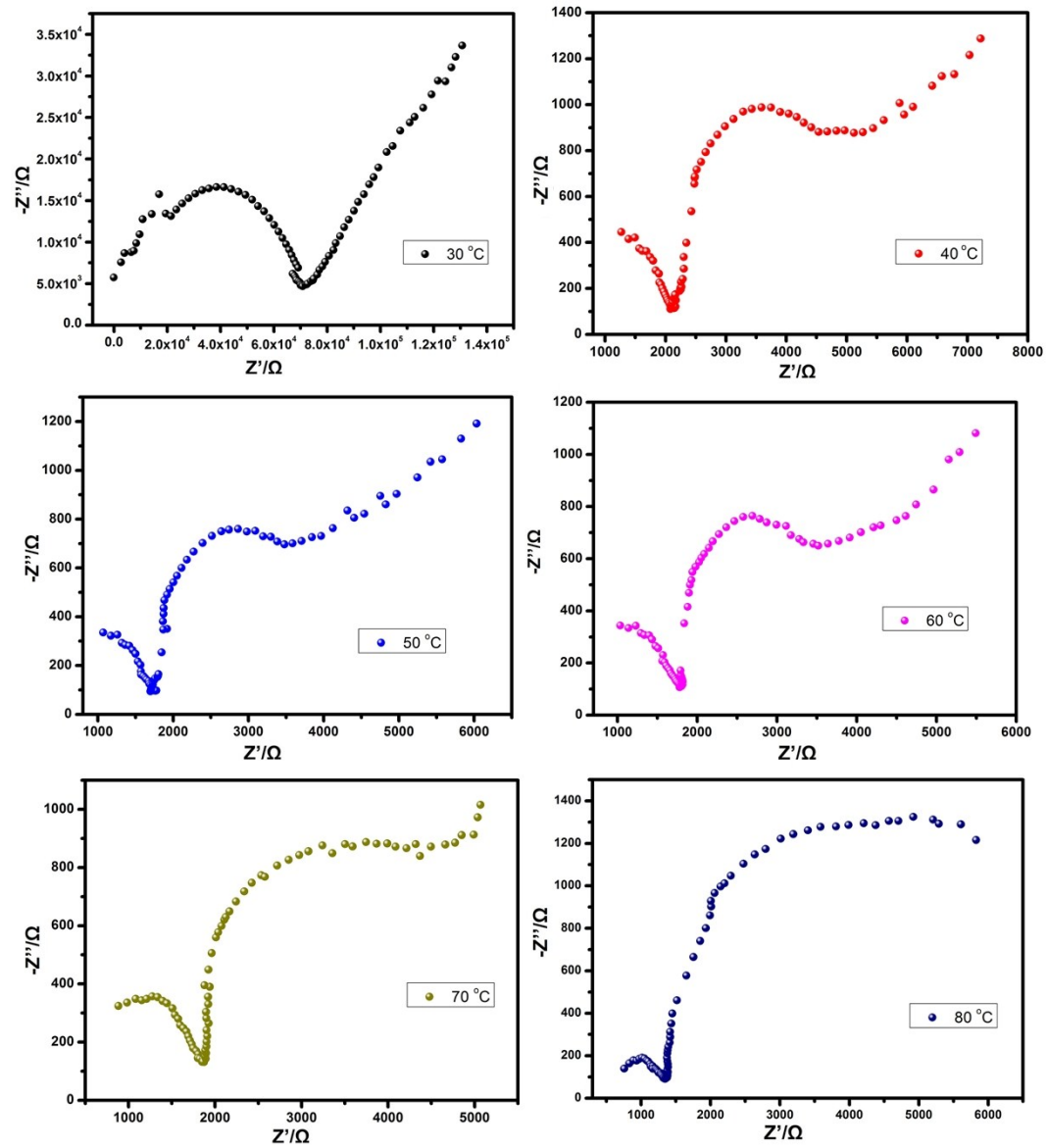


**Fig. S20** Impedance spectra of MOF-808-EDTA with 98% RH under different temperature.

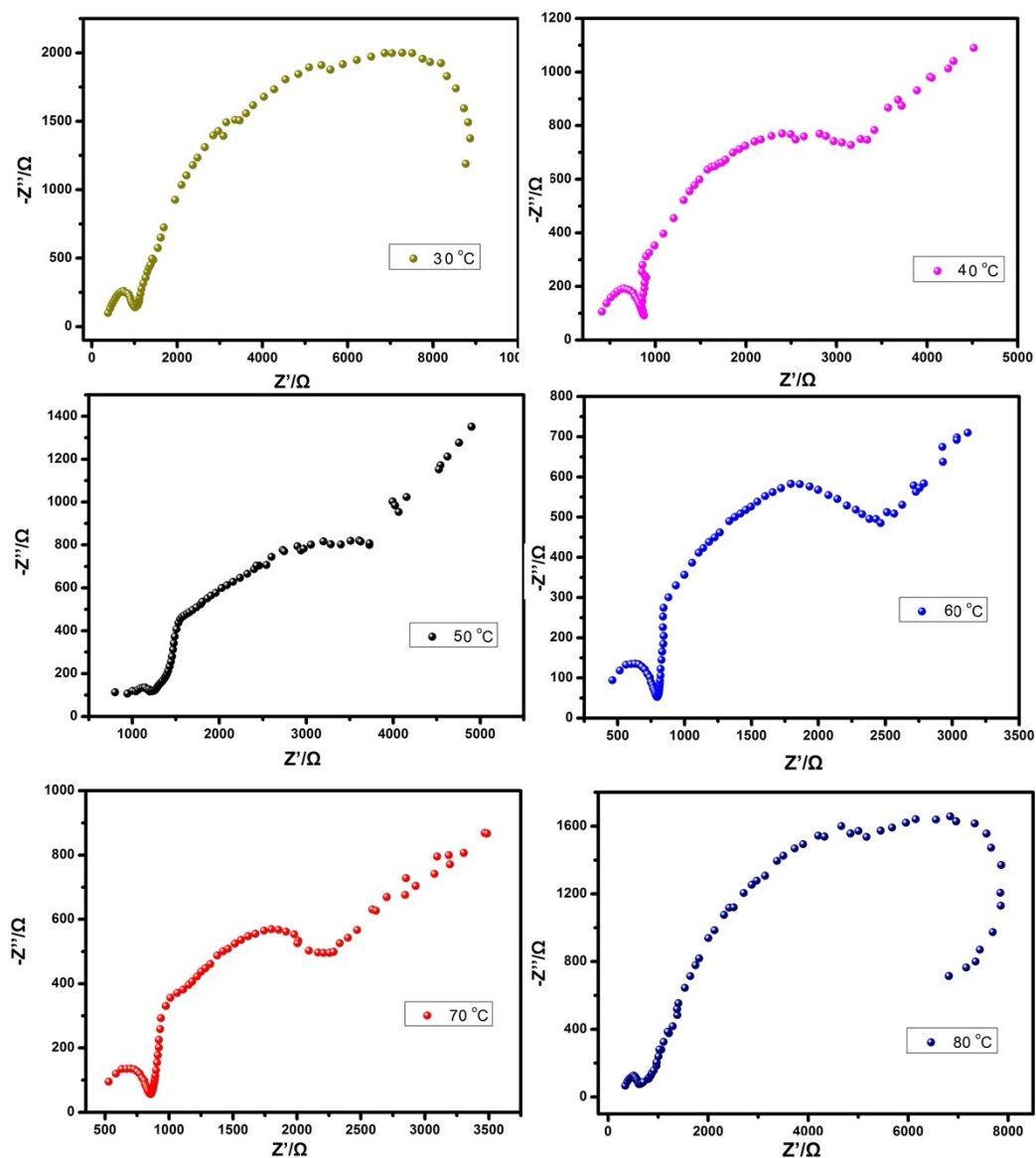


Fig. S21 Impedance spectra of MOF-808-OX with 98% RH under different temperature.

Table S2 The proton conductivities ( $\text{S cm}^{-1}$ ) of MOF-808 at 30°C with different RHs.

Relative humidity ( % )	Conductivity ( $\text{S cm}^{-1}$ )
40% RH	$1.14 \times 10^{-10}$
50% RH	$1.99 \times 10^{-10}$
60% RH	$4.34 \times 10^{-10}$
70% RH	$1.21 \times 10^{-9}$

80% RH	$4.55 \times 10^{-9}$
90% RH	$1.63 \times 10^{-8}$
95% RH	$4.86 \times 10^{-8}$
98% RH	$1.25 \times 10^{-6}$

**Table S3** The proton conductivities ( $\text{S cm}^{-1}$ ) of MOF-808 with 98% RH under different temperature.

Temperature ( $^{\circ}\text{C}$ )	Conductivity ( $\text{S cm}^{-1}$ )
30 $^{\circ}\text{C}$	$1.25 \times 10^{-6}$
40 $^{\circ}\text{C}$	$2.22 \times 10^{-6}$
50 $^{\circ}\text{C}$	$4.23 \times 10^{-6}$
60 $^{\circ}\text{C}$	$6.37 \times 10^{-6}$
70 $^{\circ}\text{C}$	$7.30 \times 10^{-6}$
80 $^{\circ}\text{C}$	$8.97 \times 10^{-6}$

**Table S4** The proton conductivities ( $\text{S cm}^{-1}$ ) of MOF-808-EDTA at 30 $^{\circ}\text{C}$  with different RHs.

Relative humidity ( % )	Conductivity ( $\text{S cm}^{-1}$ )
40% RH	$1.54 \times 10^{-10}$
50% RH	$2.47 \times 10^{-10}$
60% RH	$4.26 \times 10^{-10}$
70% RH	$9.28 \times 10^{-10}$
80% RH	$2.87 \times 10^{-9}$
90% RH	$3.54 \times 10^{-8}$
95% RH	$1.24 \times 10^{-7}$
98% RH	$1.54 \times 10^{-6}$

**Table S5** The proton conductivities ( $\text{S cm}^{-1}$ ) of MOF-808-EDTA with 98% RH under different temperature.

Temperature ( $^{\circ}\text{C}$ )	Conductivity ( $\text{S cm}^{-1}$ )
30 $^{\circ}\text{C}$	$1.54 \times 10^{-6}$
40 $^{\circ}\text{C}$	$6.63 \times 10^{-5}$
50 $^{\circ}\text{C}$	$8.62 \times 10^{-5}$
60 $^{\circ}\text{C}$	$9.80 \times 10^{-5}$
70 $^{\circ}\text{C}$	$1.04 \times 10^{-4}$
80 $^{\circ}\text{C}$	$1.31 \times 10^{-4}$

**Table S6** The proton conductivities ( $\text{S cm}^{-1}$ ) of MOF-808-OX at 30 $^{\circ}\text{C}$  with different RHs.

Relative humidity ( % )	Conductivity ( $\text{S cm}^{-1}$ )
40% RH	$5.08 \times 10^{-10}$
50% RH	$1.48 \times 10^{-9}$
60% RH	$4.99 \times 10^{-9}$
70% RH	$3.52 \times 10^{-8}$
80% RH	$5.65 \times 10^{-7}$
90% RH	$4.86 \times 10^{-6}$
95% RH	$1.37 \times 10^{-5}$
98% RH	$1.94 \times 10^{-4}$

**Table S7** The proton conductivities ( $\text{S cm}^{-1}$ ) of MOF-808-OX with 98% RH under different temperature.

Temperature ( $^{\circ}\text{C}$ )	Conductivity ( $\text{S cm}^{-1}$ )
30 $^{\circ}\text{C}$	$1.94 \times 10^{-4}$
40 $^{\circ}\text{C}$	$2.55 \times 10^{-4}$

50°C	$3.08 \times 10^{-4}$
60°C	$3.43 \times 10^{-4}$
70°C	$3.75 \times 10^{-4}$
80°C	$4.25 \times 10^{-4}$

**Table S8** Proton conductivities of selected MOFs at 298K.

Name in the Ref.	Condition	Conductivity (S cm <sup>-1</sup> )	Ref.
MFM-500(Ni)	298 K, 98% RH	$4.5 \times 10^{-4}$	3
MFM-500(Co)	298 K, 98% RH	$4.4 \times 10^{-5}$	3
LaCr, LaCo	298 K, 40–95% RH	$1 \times 10^{-6}$ - $1 \times 10^{-5}$	4
LaRu, LaLa	298 K, 40–95% RH	$3 \times 10^{-8}$	4
Li-HPAA	297 K, 98% RH	$1.1 \times 10^{-4}$	5
Cs-HPAA	292 K, 65% RH	$5.93 \times 10^{-4}$	6
PCMOF3	298 K, 98% RH	$3.5 \times 10^{-5}$	7
Ti-CAT-5	298 K, 98% RH	$8.2 \times 10^{-4}$	8
CoLa-III	298 K, 95% RH	$4.24 \times 10^{-5}$	9
(NH <sub>4</sub> ) <sub>3</sub> [Co <sub>2</sub> (bamdpH) <sub>2</sub> (HCOO)(H <sub>2</sub> O) <sub>2</sub> ]	298 K, 95% RH	$8.0 \times 10^{-6}$	10

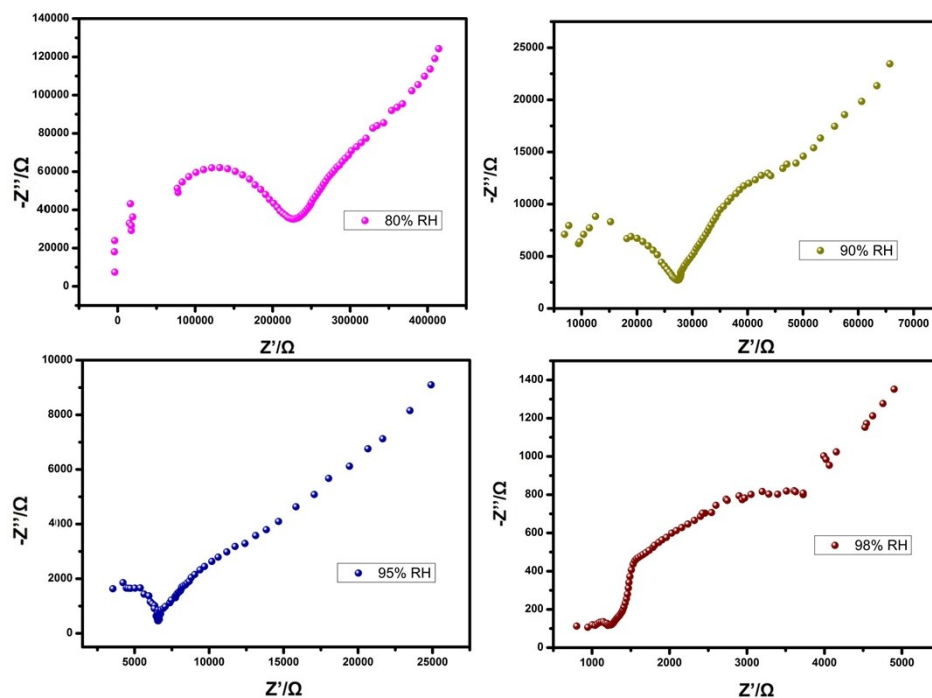


**Fig. S22** Impedance spectra of MOF-808-OX at 30 °C with different RHs.

To clarify the proton conduction pathway,  $^1\text{H-NMR-MAS}$  tests were measured with a spinning rate of 12 kHz. The water-immersed sample was prepared and ground, and then the generated powder was employed to perform this test.  $^1\text{H-NMR-MAS}$  spectra were given in the supporting information. In order to assign these present peaks, we consulted a number of literatures. The  $^1\text{H-NMR}$  spectra of three samples exhibited two similar strong peaks (Fig. S15): one wide peak located from around 6.0 to 6.7 ppm (defined as peak 1) and the other at about 2.6 ppm (peak 2). Peak 1 could be attributed to water molecules adsorbed on the sample surface and bonded with exposed functional groups via weak interactions.<sup>11-15</sup> Meanwhile, peak 2 was ascribed to  $\mu\text{-OH}$  groups connected to zirconium clusters.<sup>16</sup> Additionally, in NMR spectra of MOF-808-OX, it should be mentioned that another strong peak at approximately 0.6 ppm appears (weaker in MOF-808 and MOF-808-EDTA), resulting from mobile protons located inside the framework according to the reported literature.<sup>17</sup> Therefore, we concluded that the protons transport along the internal surfaces and nanopores in the sample.

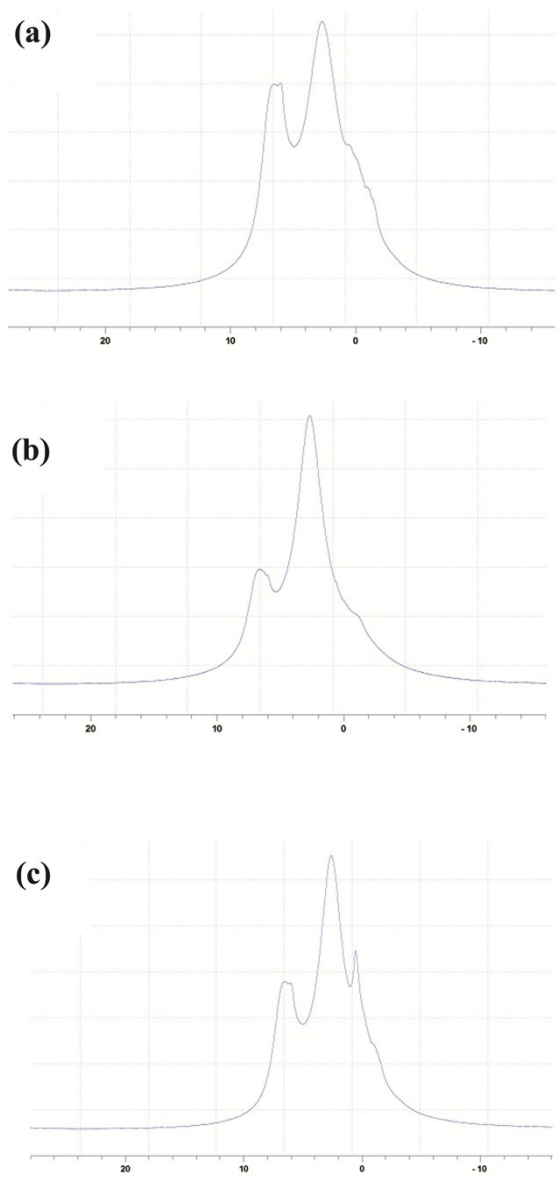


**Fig. S23** The  $^1\text{H}$ -NMR spectra of MOF-808, MOF-808-EDTA, and MOF-808-OX.

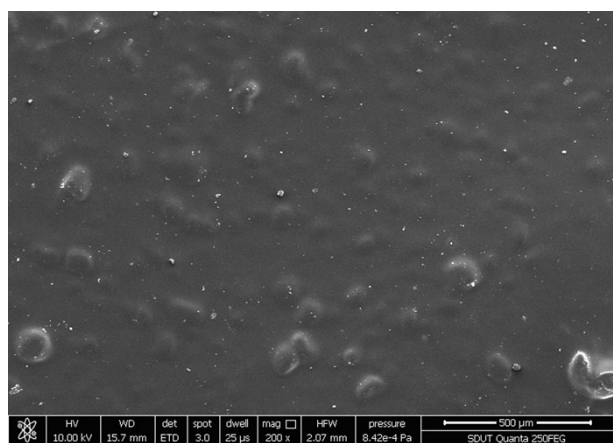


**Fig. S24** SEM image of MOF-808-OX@PVA-3 composite membrane.

**Table S9** Proton conductivities of MOF-808-OX@PVA composite membranes at different temperature.

Temperature	MOF-808-OX@PVA-7	MOF-808-OX@PVA-5	MOF-808-OX@PVA-3	MOF-808-OX@PVA-1
30 °C	$2.70 \times 10^{-6}$	$3.12 \times 10^{-6}$	$7.50 \times 10^{-6}$	$5.17 \times 10^{-6}$
40 °C	$2.88 \times 10^{-6}$	$3.66 \times 10^{-6}$	$8.05 \times 10^{-6}$	$5.96 \times 10^{-6}$
50 °C	$3.19 \times 10^{-6}$	$4.82 \times 10^{-6}$	$9.29 \times 10^{-6}$	$7.15 \times 10^{-6}$
60 °C	$3.50 \times 10^{-6}$	$5.68 \times 10^{-6}$	$1.25 \times 10^{-5}$	$8.23 \times 10^{-6}$
70 °C	$4.37 \times 10^{-6}$	$6.17 \times 10^{-6}$	$1.40 \times 10^{-5}$	$1.05 \times 10^{-5}$
80 °C	$4.75 \times 10^{-6}$	$8.20 \times 10^{-6}$	$2.03 \times 10^{-5}$	$1.43 \times 10^{-5}$

## References

1. H. Furukawa, F. Gándara, Y. B. Zhang, J. Jiang, W. L. Queen, M. R. Hudson and O. M. Yaghi, *J. Am. Chem. Soc.*, 2014, **136**, 4369.
2. Y. G. Peng, H. L. Huang, Y. X. Zhang, C. F. Kang, S. M. Chen, L. Song, D. H. Liu and C. L. Zhong, *Nat. Commun.*, 2018, **9**, 187.
3. S. Pili, S. P. Argent, C. G. Morris, P. Rought, V. Garcia-Sakai, I. P. Silverwood, T. L. Easun, M. Li, M. R. Warren, C. A. Murray, C. C. Tang, S. H. Yang and M. Schroder, *J. Am. Chem. Soc.*, 2016, **138**, 6352.
4. H. Okawa, M. Sadakiyo, K. Otsubo, K. Yoneda, T. Yamada, M. Ohba and H. Kitagawa, *Inorg. Chem.*, 2015, **54**, 8529.
5. M. Bazaga-Garcia, M. Papadaki, R. M. P. Colodrero, P. Olivera-Pastor, E. R. Losilla, B. Nieto-Ortega, M. A. G. Aranda, D. Choquesillo-Lazarte, A. Cabeza, and K. D. Demadis, *Chem. Mater.*, 2015, **27**, 424.
6. S. J. Liu, C. Cao, F. Yang, M. H. Yu, S. L. Yao, T. F. Zheng, W. W. He, H. X. Zhao, T. L. Hu and X. H. Bu, *Cryst. Growth. Des.*, 2016, **16**, 6776.
7. J. M. Taylor, R. K. Mah, I. L. Moudrakovski, C. I. Ratcliffe, R. Vaidhyanathan and G. K. H. Shimizu, *J. Am. Chem. Soc.*, 2010, **132**, 14055.
8. T. N. Tu, N. Q. Phan, T. T. Vu, H. L. Nguyen, K. E. Cordova and H. Furukawa, *J. Mater. Chem. A*, 2016, **4**, 3638.

9. S. S. Bao, K. Otsubo, J. M. Taylor, Z. Jiang, L. M. Zheng and H. Kitagawa, *J. Am. Chem. Soc.*, 2014, **136**, 9292.
10. Z. S. Cai, S. S. Bao, X. Z. Wang, Z. Hu and L. M. Zheng, *Inorg. Chem.*, 2016, **55**, 3706.
11. S. Kim, H. J. Avila-Paredes, S. Wang, C.-T. Chen, R. A. De Souza, M. Martin and Z. A. Munir, *Phys. Chem. Chem. Phys.*, 2009, **11**, 3035.
12. B. Grünberg, T. Emmler, E. Gedat, I. Shenderovich, G. Findenegg, H.-H. Limbach and G. Buntkowsky, *Chem. Eur. J.*, 2004, **10**, 5689.
13. J. Soria, J. Sanz, I. Sobrados, J. Coronado, A. Maira, M. Herández-Alonso and F. Fresno, *J. Phys. Chem. C*, 2007, **111**, 10590.
14. H. E. Gottlieb, V. Kotlyar and A. Nudelman, *J. Org. Chem.*, 1997, **62**, 7512.
15. H. J. Avila-Paredes, E. Barrera-Calva, H. U. Anderson, R. A. De Souza, M. Martin, Z. A. Munir and S. Kim, *J. Mater. Chem.*, 2010, **20**, 6235.
16. C. A. Trickett, T. M. O. Popp, J. Su, C. Yan, J. Weisberg, A. Huq, P. Urban, J. Jiang, M. J. Kalmutzki, Q. Liu, J. Bae, M. P. Head-Gordon, G. A. Somorjai, J. A. Reimer and O. M. Yaghi, *Nature Chem.*, 2019, **11**, 170.
17. J. Hinterberg, A. Adams, B. Blümich, Paul Heitjans, S. Kim, Z. A. Munir and M. Martin, *Phys. Chem. Chem. Phys.*, 2013, **15**, 19825.